Desalination 616 (2025) 119395

Contents lists available at ScienceDirect

Desalination

journal homepage: www.elsevier.com/locate/desal

Efficient lithium extraction from salt lakes brine via regulating the electric double-layer interface of high-loading film electrodes with CMC—Li

Yawen Gao [a], Luxiang Ma [a,*], Xin Zeng [a], Zhixiang Li [a], Ting Li [a], Chunxi Hai [a], Tiandong Chen [a], Yanxia Sun [a], Shengde Dong [a], Xin He [a], Qi Xu [a], Xiaowang Wu [c], Hongli Su [b], Yuan Zhou [a]

[a] College of Materials and Chemistry & Chemical Engineering, Cheng Du University of Technology, Cheng Du, 610059, PR China
[b] Resource & Recycling, Department of Engineering Structures, Faculty of Civil Engineering and Geosciences, Delft University of Technology, Delft, 2628, CN, the Netherlands
[c] Qinghai Zhongxin Guoan Lithium Development Co., LTD., Qinghai Key Laboratory of Comprehensive Utilization of sulfate salt lake resources, Ge Er Mu, 816000, PR China

HIGHLIGHTS

- A double electric layer interface engineering strategy is proposed to drive the efficient migration of lithium ions.
- CMC-Li significantly enhances the wettability of film electrodes.
- CMC-Li LFP effectively reduces the Mg/Li ratio in low-grade brine.

GRAPHICAL ABSTRACT

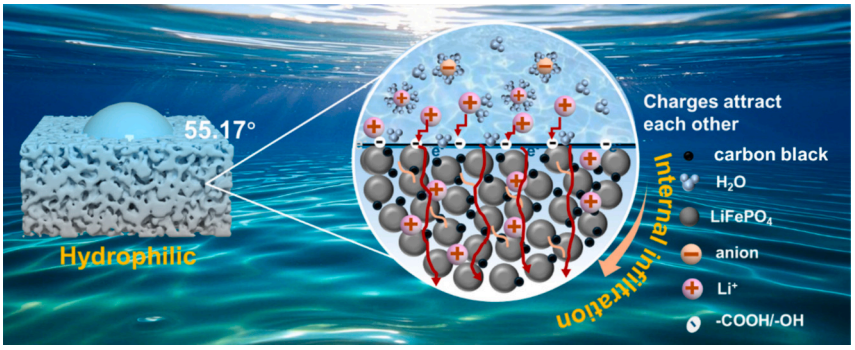

ARTICLE INFO

Keywords:
Lithium extraction
Electrochemical de-lithiation method
High loaded film electrode
Hydrophilic
Electric double layer

ABSTRACT

In response to the problems of large interfacial diffusion resistance and low lithium extraction efficiency in traditional high-loading film electrodes during lithium extraction from salt lakes by the electrochemical de-intercalation method, this paper presents an interfacial engineering strategy based on the carboxymethyl cellulose lithium (CMC—Li) binder. By modulating the structure of the inner Helmholtz plane (IHP) of the electrical double layer and enlarging the effective specific surface area, the migration rate of Li^+ and the lithium extraction efficiency are remarkably enhanced.

In this study, a CMC-Li composite electrode sheet was prepared using Spent $LiFePO_4$ as the raw material. It was demonstrated that the carboxyl (-COOH) and hydroxyl (-OH) functional groups of CMC-Li can be directionally adsorbed on the electrode surface. This adsorption event reconstructs the IHP-layer structure, reduces the solvation energy barrier of Li^+, and increases the effective specific surface area of the film electrode. As a result, the contact angle decreased from 130.01° to 55.17°. Furthermore, in the CMC-Li system, the lithium extraction rate in simulated brine increased from 0.33 $mg{\cdot}g^{-1}{\cdot}min^{-1}$ to 0.69 $mg{\cdot}g^{-1}{\cdot}min^{-1}$, while the energy consumption decreased by a factor of 3. In the West Taijinar brine, the lithium extraction capacity reached 23.01 $mg{\cdot}g^{-1}$ with

* Corresponding author.
E-mail address: maluxiang@cdut.edu.cn (L. Ma).

https://doi.org/10.1016/j.desal.2025.119395
Received 18 June 2025; Received in revised form 5 September 2025; Accepted 7 September 2025
Available online 8 September 2025

a concurrent dramatic reduction in the Mg/Li ratio from 141 to 0.42. These results indicate that the CMC-Li system exhibits excellent lithium extraction performance and high selectivity. Overall, this study proposes a groundbreaking interfacial design concept that achieves both high efficiency and sustainability for lithium extraction from salt lake brines.

1. Introduction

Lithium, recognized as a strategically critical mineral, plays a pivotal role in diverse industries including new energy, glass-ceramics, pharmaceuticals, and aerospace engineering [1,2]. The exponential growth of electric vehicle powered by lithium-ion batteries has significantly escalated global lithium demand. As a result, the development of efficient lithium extraction technologies has emerged as a pressing issue in both academic and industrial communities [3]. Approximately 70 % of global lithium reserves are hosted in salt lake brines, surpassing those in hard rock ores and seawater [4]. Compared to environmentally intensive ore processing and low-yield seawater extraction, brine-based lithium recovery offers distinct advantages in cost-effectiveness and environmental sustainability, making it the dominant approach for lithium production [5,6].

Electrochemical de-intercalation has garnered substantial attention due to its dual benefits of high Li^+ selectivity and adaptability to brines with varying salinities [7,8]. This technology operates similarly to lithium-ion batteries, utilizing brine as the electrolyte and paired electrodes (lithium-rich anode and lithium-deficient cathode) to selectively extract Li^+ under controlled potentials [9]. In this approach, the active materials (e.g., $LiMn_2O_4$, $LiFePO_4$) serve as the key components that participate directly in the electrochemical reactions, facilitating the intercalation and deintercalation of Li^+. These processes are primarily driven by reversible redox reactions. Therefore, to enhance the adsorption capacity, the loading of active material in the film electrode should be significantly higher than that in conventional lithium-ion battery electrodes [10]. Moreover, the film electrode must be immersed in highly viscous and calcified brine for extended periods. The unique structure and operating environment of the film electrode results in low lithium extraction efficiency, limiting its large-scale commercial application. Therefore, designing high-loading thick electrodes by increasing active material content can significantly enhance Li^+ adsorption efficiency per unit area [11,12]. Our research team proposed a strategy of constructing a three-dimensional conductive network thick electrode using reduced graphene oxide, biochar, and melamine-formaldehyde resin (MF), which significantly increases the electrical conductivity, alleviates electrochemical polarization, and improves the lithium extraction capacity [13,14].

However, with the increase of the load of active materials and the thickness of the film electrode, in large-area, high-loading film electrodes, the extended charge transfer paths, reduced porosity, and strong hydrophobicity of both carbon materials and conventional binders significantly reduce the brine's wettability on the electrode surface, thereby effectively suppressing the diffusion rate of brine within the electrode. Consequently, the lithium adsorption efficiency per unit area is reduced. To address the issues of slow diffusion or diffusion in high-loading film electrodes, Xu et al. [15] employed a salt-templating method to create pores in the electrode and introduced polyethylene glycol (PEG) to improve the electrode's hydrophilicity and diffusion channels. However, while pore-formation enhanced brine wettability, it led to the loss of some active materials. Luo et al. [16] constructed an electrochemical system for lithium extraction from salt lakes using ZnO-coated $LiMn_2O_4$. This not only improved the material's hydrophilicity but also exhibited good selectivity for Li^+. However, ZnO is an electrochemically inactive electrode material, and the interfacial modification strategy is not favorable for Li^+ migration. Our research group proposed a sulfonation strategy and fabricated a high-loading film electrode (45 $mg{\cdot}cm^{-2}$) using sulfonated PVDF as the binder, which enhanced the electrode's wettability in salt lake brine and increased the efficiency of lithium extraction [17]. However, polyvinylidene fluoride (PVDF), as a conventional binder used in lithium-ion battery electrodes, undergoes severe swelling during prolonged exposure to brine, which leads to reduced adhesion and detachment of active materials. Additionally, the sulfonation process is relatively complex and costly, posing challenges for large-scale commercial application. Therefore, it is essential to develop new strategies to simultaneously address the challenges of adsorption capacity and adhesion in high-loading film electrodes.

The interfacial structure of film electrodes largely determines the extent and efficiency of interactions between electrode materials and brine, thereby influencing Li^+ transport efficiency. During lithium extraction in salt lake brine using film electrodes, Li^+ ions undergo a hydration process upon approaching the electrode surface. Subsequently, they traverse the electrical double layer (EDL) at the electrode/brine interface and intercalate into the electrode material. The EDL consists primarily of the inner Helmholtz layer (IHL) and the outer Helmholtz layer (OHL) [18]. Regarding the investigation of how electric double layer (EDL) modulation affects Li^+ intercalation and migration, existing research has established a solid foundation. Cheng et al. [19] proposed that the solvation structure of ions at electrochemical interfaces is a critical factor governing ion-electrode interactions. When solvation is weak, it helps ions penetrate the internal Helmholtz plane (IHP) and enter the interior of the electrode. Hu et al. [20] further elucidated the influence of anions (NO_3^-, Cl^-, SO_4^{2-}, and CH_3COO^-) on solid-liquid interface reconstruction and Li^+ transport across the Helmholtz plane, demonstrating that the physical properties of anions are closely tied to Li^+ interfacial transport. Therefore, leveraging anion-specific adsorption at the Helmholtz plane and by introducing anions to alter the solvation state of ions within the IHP, can accelerate the entry of brine ions into the electrode surface. This approach not only enhances the effective contact area between the film electrode and brine but also significantly improves electrochemical reaction efficiency, ultimately boosting lithium extraction performance [20].

Lithium carboxymethyl cellulose (CMC—Li), an aqueous conductive polymer binder, finds extensive applications in battery technologies. For instance, Shin et al. [21]developed high-performance all-solid-state batteries (ASSBs) by incorporating CMC-Li as a conductive binder, thereby enhancing interfacial conductivity. Current research on this binder primarily focuses on its migration rate and conductivity within batteries. However, few studies have explored the impact of CMC-Li on the electric double layer (EDL) at the brine/film-electrode interface in lithium extraction from salt lakes. Among them, CMC-Li is rich in anionic functional groups, such as -COOH and -OH. Under the action of an external electric field, CMC-Li can effectively regulate the structure of EDL, enhance the electrostatic attraction between the electrode and Li^+, reduce the hydration degree of Li^+, and increase the effective contact area between the film electrode and the brine. These effects jointly reduce the diffusion energy barrier of Li^+ and enhance the lithium extraction capacity of the high-load film electrode. Therefore, in this work, the film electrode is regarded as a whole. Not only is the internal Li^+ transport studied, but also the interface regulGation of the film electrode by CMC-Li is investigated starting from the mass transfer process at the interface between the film electrode and the brine, thereby enhancing the capacity.

Therefore, this study proposes an interfacial engineering strategy based on the carboxymethyl cellulose lithium (CMC—Li) binder. By introducing anionic groups (-COOH, -OH), the solvation state of ions at the inner Helmholtz plane is altered, the effective specific surface area

between the film electrode and brine is increased, the migration rate of Li^+ is enhanced, and consequently, the lithium extraction efficiency is improved. The research process is shown in Fig. 1. CMC-Na undergoes cation exchange at 15 wt% p-toluenesulfonic acid (TsOH) to obtain CMC—H. Subsequently, CMC-Li was obtained by reaction in 7 wt% lithium hydroxide (LiOH) solution. The Li^+ content in the film electrode is 18.8 $mg{\cdot}g^{-1}$. In addition, a CMC-Li LFP/CMC-Li FP system was constructed for lithium extraction by electrochemical intercalation and de-intercalation, and its performance comprehensively compared to conventional LFP electrodes. It was demonstrated that CMC-Li $LiFePO_4$ (CMC-Li LFP) exhibits excellent hydrophilicity, Li^+ migration rate, and lithium extraction performance. This method provides a novel idea for the development of thick electrodes for highly efficient lithium extraction.

2. Results and discussion

2.1. Structure and morphology characterization of materials

The functional group structures of the three samples prepared were observed by Fourier Transform Infrared spectroscopy (FT-IR), as shown in Fig. 2a. The characteristic peaks corresponding to -OH (stretching vibration within 3600–3000 cm^{-1}), C—H (stretching vibration at 2960 cm^{-1}), and —O— (stretching vibration at 1032 cm^{-1}) of the three samples were basically the same, indicating that the original structure of CMC was not damaged through two-step cation exchange [21]. **Fig. S2** further confirms this point. Furthermore, CMC-H exhibits a new characteristic peak -COOH at 1731 cm^{-1}, indicating that Na^+ and H^+ undergo exchange and Na^+ disappears. After Li^+ exchange, the FT-IR spectrum of CMC-Li was similar to that of CMC—Na, the -COOH group disappeared, and CMC-Li was successfully obtained. Meanwhile, a systematic investigation on the composition of the binder was conducted by fabricating film electrodes with CMC—Li: SBR mass ratios of 1:1, 2:1, and 2.5:1.5. As shown in **Fig. S1**, the film electrode with a CMC—Li: SBR ratio of 2.5:1.5 was selected for a comparative performance study with the conventional PVDF LFP film electrode. The chemical structure and elemental content of CMC samples, as well as CMC-Li LFP and PVDF LFP, were analyzed by X-ray photoelectron spectroscopy (XPS). As shown in Fig. 2b-c, CMC-Na has a Na 1 s peak but no Li 1 s peak. In CMC—Li, there is a Li 1 s peak but no Na 1 s peak, indicating that CMC-Li was successfully prepared after two cation reactions. Furthermore, in the C 1 s spectra of CMC-Li LFP and PVDF LFP (Fig. 2d), due to the presence of PVDF, the original LFP shows the F-C-F peak, the C—O peak at 286.5 eV indicates the presence of a small amount of NMP on the electrode surface. While CMC-Li LFP has the -COOH, -OH and -C-O-C peaks. The above results confirm the successful preparation of CMC—Li. Furthermore, nano-scratch tests were carried out on PVDF LFP and CMC- Li LFP electrode sheets with a loading of 18.8 $mg{\cdot}cm^{-2}$, respectively. As shown in Fig. 2e-f, with the increase of the load force value, compared with the PVDF LFP electrode sheet, the CMC-Li LFP electrode sheet had higher hardness and adhesion.

Scanning electron microscopy (SEM) was employed to analyze the surface morphologies of CMC—Na, CMC—Li, and their corresponding electrode sheets. As depicted in Fig. 3a-d, both CMC-Na and CMC-Li exhibited a strip-shaped hollow- tube structure, indicating that the morphology remained unchanged after the ion-exchange process. Moreover, energy-dispersive X-ray spectroscopy (EDS) elemental mapping confirmed the absence of Na elements in the CMC-Li powder, signifying the successful conversion of CMC-Na to CMC-Li (Fig. 3e-g). The cross-section of CMC-Li LFP, as shown in Fig. 3h, revealed that the thickness of the active material was 87.1 μm, and the areal loading of the thick electrode was 18.8 $mg{\cdot}cm^{-2}$. Furthermore, as presented in Fig. 3i-l, following electrode slurry processing and coating, the ribbon-like structure of CMC-Li is transformed into granular morphology due to physical segmentation by carbon black particles during forced dispersion. In addition, since CMC-Li is a water-based binder with better dispersibility and malleability, when combined with SBR to form the binder, the fibrous structures aggregate to create a fine particulate network, it is more conducive to the formation of a network structure between the binder and the electrode material [21]. Thus, compared with the traditional PVDF LFP, the CMC-Li LFP electrode sheet featured denser particles without cracks. Additionally, the distribution among the electrode particles, conductive agents, and the binder was relatively uniform, and the voids between the particles were also more uniform, without the severe particle agglomeration phenomenon observed in Fig. 3l.

Building upon the analysis conducted via scanning electron microscopy, a further investigation was carried out regarding the internal pores of the electrodes and their degree of wetting. As illustrated in Fig. 4a-c, the nitrogen physical adsorption-desorption isotherms of both

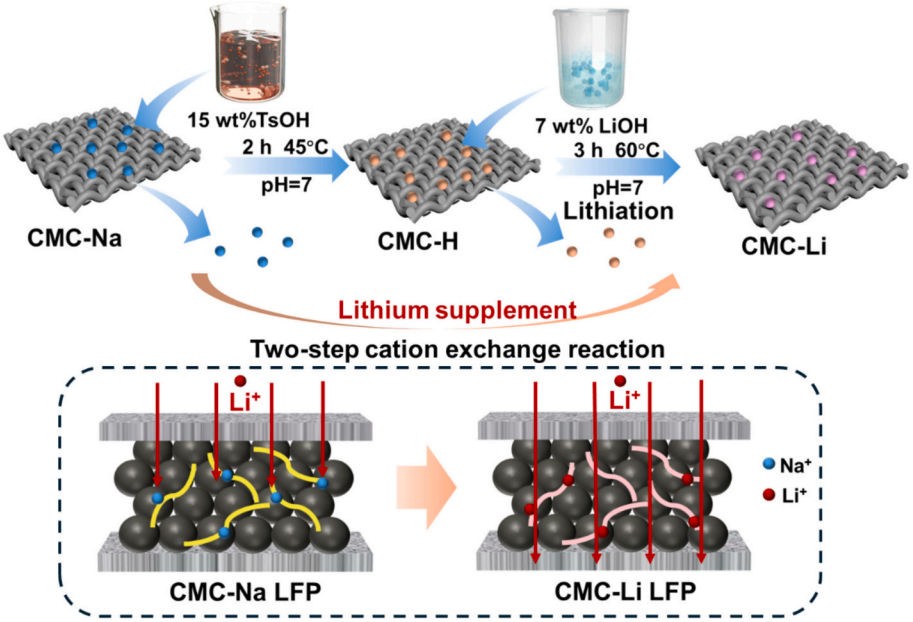

Fig. 1. Preparation process diagram of CMC—Li.

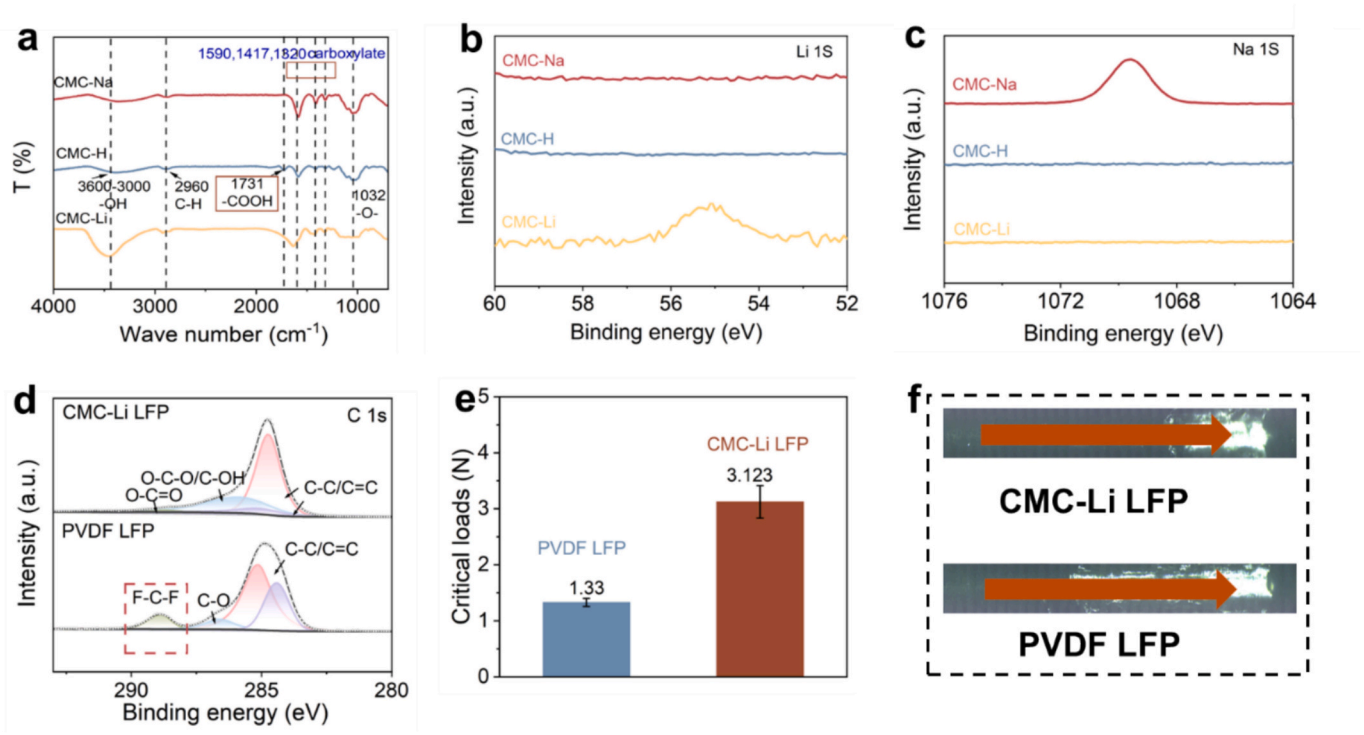

Fig. 2. XPS and Infrared spectra of the samples. (a) Infrared spectra of the samples; high-resolution spectra of (b) Li 1 s and (c)Na 1 s; (d)C 1 s of CMC-Li LFP and PVDF LFP; (e) Binding force of PVDF LFP and CMC-Li LFP; (f) Indentation simulation image of the samples.

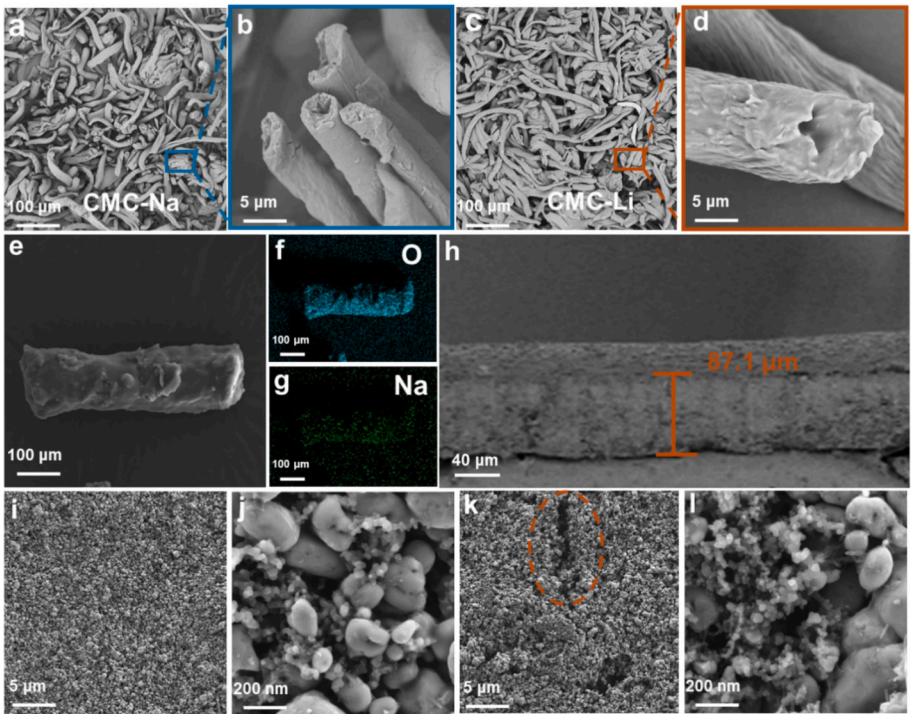

Fig. 3. Morphology and contact Angle characterization of samples. SEM images of (a-b) CMC—Na, (c-d) CMC—Li, (e-g) EDS of CMC—Li, (h) Cross section of CMC-Li LFP, (i-j) CMC-Li LFP, (k-l) PVDF LFP.

PVDF LFP and CMC-Li LFP belong to Type IV, with an adsorption hysteresis loop appearing at high pressures [22]. In comparison to PVDF LFP, CMC-Li LFP exhibits a higher specific surface area, measuring 30.72 $m^2 \cdot g^{-1}$ and 20.35 $m^2 \cdot g^{-1}$, respectively. Additionally, the particle voids of CMC-Li LFP are more uniform, with an average void size of 9.8557 nm, indicating that this electrode has larger particle voids compared to the original electrode.

Moreover, the contact angles of PVDF-LFP and CMC-Li-LFP in the West Taijinar brine are compared through multiple repeated experiments by comparing the Wettability of PVDF LFP and CMC-Li LFP in the

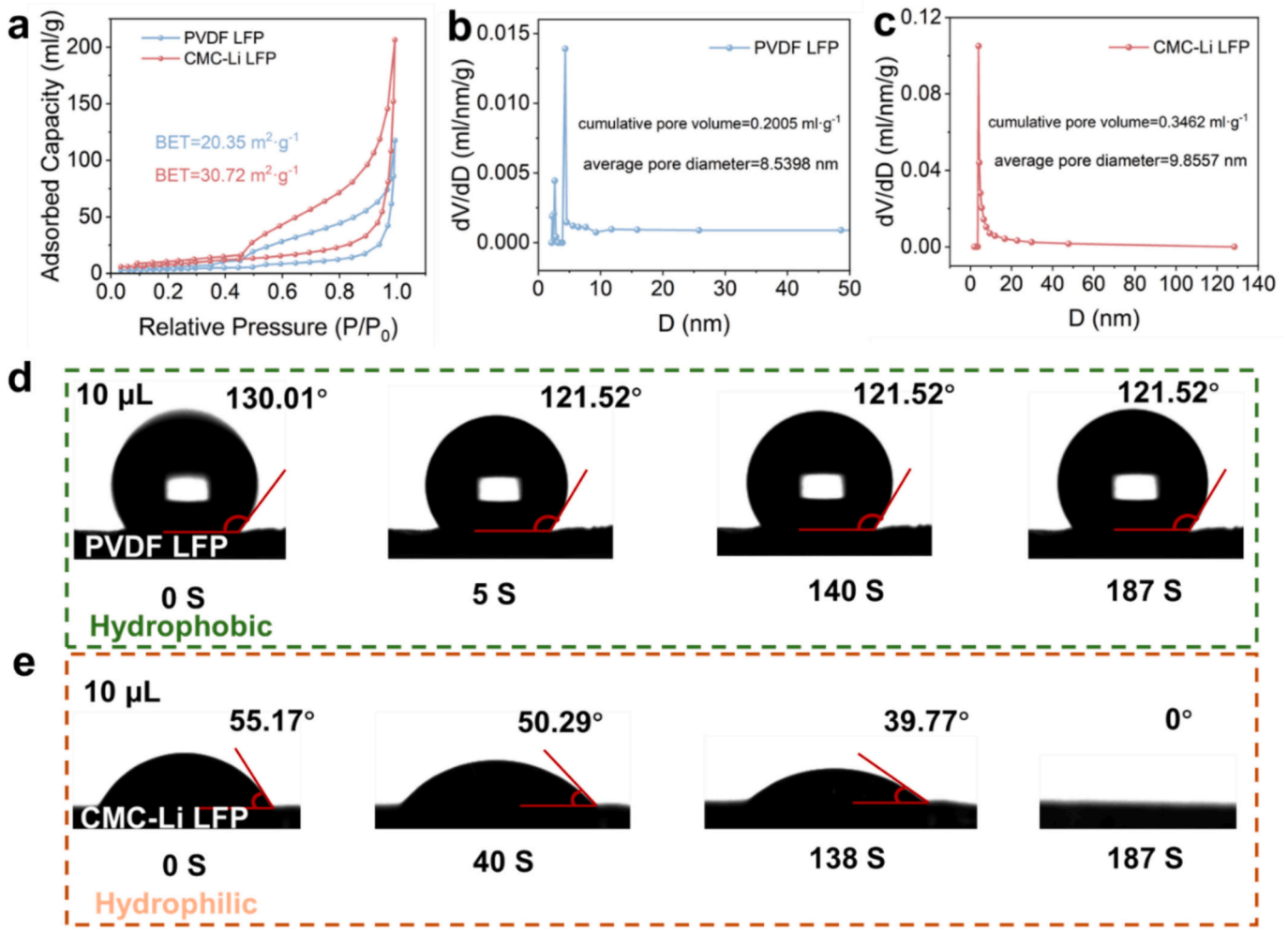

Fig. 4. Specific surface area test and contact Angle analysis of PVDF LFP and CMC-Li LFP. (a) Adsorption-desorption isotherm; (b-c) BJH pore size and volume analysis; (d-e) contact Angle.

West Taijinar brine (Fig. 4d-e **and Fig.S3**), it is evident that PVDF LFP shows remarkable hydrophobicity with a contact angle of 130.01° under the same droplet conditions and time. Even after three minutes of penetration, the degree of droplet wetting remains essentially unchanged. On the contrary, CMC-Li LFP demonstrates significant hydrophilicity right from the start (at 0 s) with a contact angle of 55.17°. After three minutes of penetration, the droplet is nearly completely wet, and the penetration rate is 3.22 μL·min^{-1}. The above results indicate that CMC-Li LFP has high porosity and good wettability. According to **Eq. (1)**, it can be seen that when the film electrode is completely immersed in the brine of the salt lake, increasing the porosity to enhance the infiltration degree between the brine and the electrode can effectively strengthen the diffusion process of the brine in the electrode, thereby increasing the migration speed of lithium ions in the film electrode and improving the efficiency of lithium extraction.

$$D_{\text{eff}} = \frac{\varepsilon}{\tau} D_0 \tag{1}$$

where ε represents porosity, τ denotes tortuosity, and D_0 is the diffusion coefficient of Li^+ in the brine [23].

2.2. Electrochemical properties of CMC-Li LFP and PVDF LFP

The Li^+ transport process at the brine-electrode interface is illustrated in Fig. 5a. When brine contacts the electrode surface, the charged electrode surface attracts counter-ions from the electrolyte, forming a charge distribution region near the electrode surface. This typically consists of the inner Helmholtz plane (IHP) and outer Helmholtz plane (OHP), constituting the electrical double layer (EDL) structure [24]. This configuration is commonly represented using equivalent circuit modeling of electrochemical impedance spectroscopy, providing insights into the kinetic behavior of the film electrode in brine environments. As depicted in Fig. 5b-c, the electrochemical impedance equivalent-circuit simulation reflects the reaction kinetics of the film electrode in brine. Rs and Rct represent the migration resistance of Li^+ in brine and the charge-transfer resistance at the film-electrode interface, respectively. Compared with PVDF LFP, CMC-Li LFP exhibits smaller Rs (3.04 Ω) and Rct (0.21 Ω) values, indicating that CMC-Li LFP has a faster electrode-reaction rate and electron-transfer ability [25]. Additionally, W represents the diffusion process of Li^+ at the electrode interface. In contrast to the traditional electrode, the diffusion resistance of CMC-Li LFP was significantly reduced to 1.78 Ω, which remarkably enhanced the diffusion of Li^+, thereby improving the lithium extraction performance.

The cyclic voltammetry (CV) curves of CMC-Li LFP and PVDF LFP at 0.2 mV·s^{-1} are presented in Fig. 5d. Compared with PVDF LFP, CMC-Li LFP has a higher peak- current value and a smaller redox-potential difference (0.188 V) than PVDF LFP (0.249 V), suggesting that CMC-Li LFP has less polarization. Fig. 5e shows the performance rate of the electrodes in the range of 0.1 to 3C. The discharge capacities of all three materials decrease with the increase in the rate. However, CMC-Li LFP maintains a higher discharge capacity than PVDF LFP at each rate. Even

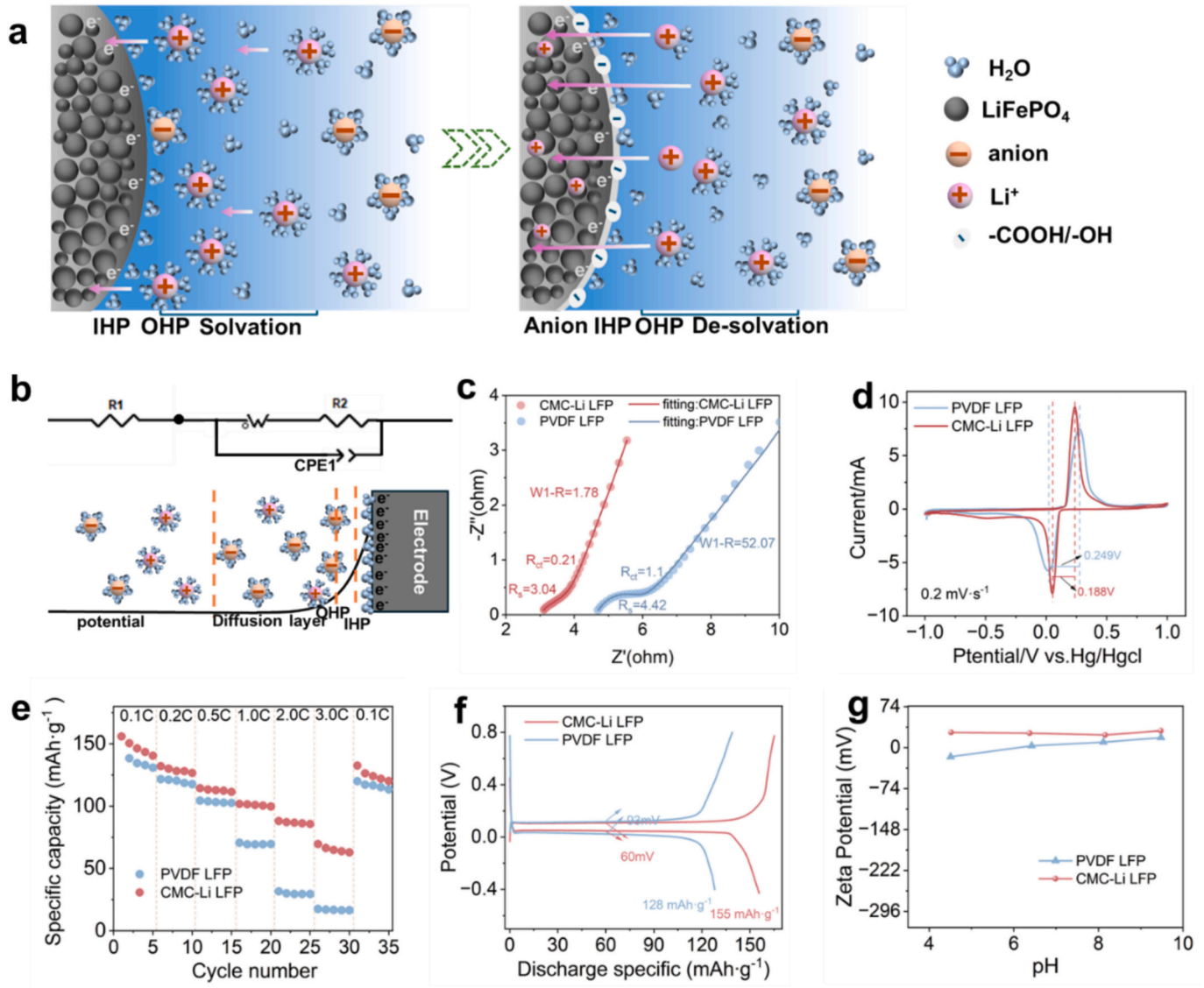

Fig. 5. (a)Schematic diagram of anion migration of Li^+ from brine to electrode interface. Electrochemical tests of CMC-Li LFP and PVDF LFP electrode; (b)Impedance analog circuit diagram; (c)EIS in 0.5 M LiCl; (d)Circular voltametric test curve at 0.2 $mV{\cdot}s^{-1}$; (e)Discharge capacity at different rates in 0.1 M LiCl; (f)The charge/discharge curves in 0.1 M LiCl; (g)zeta potential diagram.

at a high rate of 3C, the specific discharge capacity of CMC-Li LFP (69.5 $mAh{\cdot}g^{-1}$) is significantly higher than that of PVDF LFP (26 $mAh{\cdot}g^{-1}$). Furthermore, when the rate decreased to 0.1C, the initial capacity of the CMC-Li LFP electrode recovered substantially to 132.5 $mAh{\cdot}g^{-1}$. This indicates that the film electrode exhibits excellent reversibility and structural stability.

The long-term cycling performance of CMC-Li LFP at 0.2C is presented in **Fig. S4**. Compared to PVDF LFP, the CMC-Li LFP electrode delivers a significantly higher initial discharge capacity of 157.1 $mAh{\cdot}g^{-1}$. Furthermore, after 50 cycles, it exhibits markedly enhanced capacity retention, confirming its superior cycling stability. Charge–discharge profiles of both CMC-Li LFP and PVDF LFP were also measured (Fig. 5f). A relatively flat voltage plateau is observed around 0.15 V. Compared to PVDF LFP (93 mV), the CMC-Li LFP electrode shows lower polarization (60 mV) and higher charge/discharge capacities. This improvement can be attributed to the additional Li^+ ions supplied by CMC—Li, which reduce the diffusion energy barrier for Li^+, facilitate dehydration, and enhance Li^+ transport kinetics. These results further demonstrate faster lithium-ion migration within the CMC-Li LFP composite and underscore its promising electrochemical performance [26].

Moreover, the introduction of CMC-Li markedly enhances the Li^+ selectivity of the LFP electrode. As illustrated in Fig. 5, at pH 6.3 (reflects the typical environment of salt lake brine), the CMC-Li LFP composite exhibits a higher net positive surface charge compared to the conventional PVDF LFP. This behavior stems from the inherent positive surface charge of $LiFePO_4$ under these conditions. Although CMC itself carries a negative charge, its low concentration as a binder, together with the presence of Li^+ ions that further mitigate negative contributions, results in the overall dominance of positive surface characteristics. Consequently, the CMC-Li modified LFP displays a more pronounced net positive charge. While a positively charged surface generally repels cations electrostatically, the low concentration of Li^+ (140 ppm) and its low charge density allow Li^+ ions to overcome this repulsion under an applied electric field and be adsoallowsonto the electrode surface. In contrast, Mg^{2+} ions exist at significantly higher concentrations (20,010 ppm) and possess a higher charge density, leading to strong electrostatic repulsion. This stark difference in interaction underpins the excellent Li^+/Mg^{2+} selectivity of the CMC-Li modified LFP electrode, demonstrating its high potential for efficient magnesium-lithium separation

[20,27].

2.3. Study on Lithium extraction performance of CMC-Li LFP/CMC-Li FP and PVDF LFP/PVDF FP Systems in Brine

Based on electrochemical performance, study on the lithium extraction capacity of the CMC-Li LFP/CMC-Li FP system in pure lithium solution, simulated brine, the West Taijinar brine and the lithium extraction capacity in the West Taijinar old brine. Fig. 6a shows the lithium extraction device using the electrochemical deintercalation method in this study. Under the action of voltage, CMC-Li LFP and CMC-Li FP in this system undergo redox reactions respectively in brine (as shown in the electrode reaction equations in Fig. 6a), thereby realizing the reversible deintercalation and intercalation of lithium ions in the electrode matrix.

On this basis, the lithium-extraction performance of the two systems in the pure LiCl lithium solution was first studied. As shown in Fig. 6b, at a voltage of 0.8 V, with the increase of time, the lithium content in the three systems gradually increased. Compared with PVDF LFP, the CMC-Li LFP electrode not only had a significant increase in lithium-extraction content, reaching 42.8 $mg{\cdot}g^{-1}$, but also had a faster lithium-extraction rate. At around 60 min, the lithium-extraction amount of CMC-Li LFP basically stabilized at 39.9 $mg{\cdot}g^{-1}$, while that of PVDF LFP was only 23.9 $mg{\cdot}g^{-1}$, and the lithium-extraction of PVDF LFP basically stabilized at around 90 min. The relationship between voltage and time in **Fig. S5** further demonstrated that CMC-Li LFP had a faster lithium-extraction rate. Compared with PVDF LFP, the voltage of CMC-Li LFP tended to be stable at around 57 min. In addition, after 5 cycles, the change in lithium - release capacity each time was small (Fig. 6c), and the average lithium capacity (41.54 $mg{\cdot}g^{-1}$was higher than the average lithium capacities of PVDF LFP (36.87 $mg{\cdot}g^{-1}$) and CMC-Na LFP (39.25 $mg{\cdot}g^{-1}$). Additionally, the energy consumption of CMC-Li LFP and PVDF LFP was calculated according to **Eq. (2).** The energy consumption of the entire lithium-extraction process was only 4.195 $Wh{\cdot}mol^{-1}$ and the intercalation rate of Li^+ in the CMC-Li LFP/CMC-Li FP system was 0.685 $mg{\cdot}g^{-1}{\cdot}min^{-1}$. Compared with PVDF LFP (0.325 $mg{\cdot}g^{-1}{\cdot}min^{-1}$), the rate was approximately doubled, and the energy consumption was reduced by about 3 times (Fig. 6d-e). The above results indicate that the CMC-Li LFP/CMC-Li FP system has better lithium-extraction performance.

$$E_{sec} = \frac{M_{Li}{\cdot}U{\cdot}\int_0^t I_0(t)dt}{3.6E_{Li}{\cdot}w} \tag{2}$$

where E_{sec} is specific energy consumption [$Wh{\cdot}mol^{-1}$]; M_{Li} Is the molar

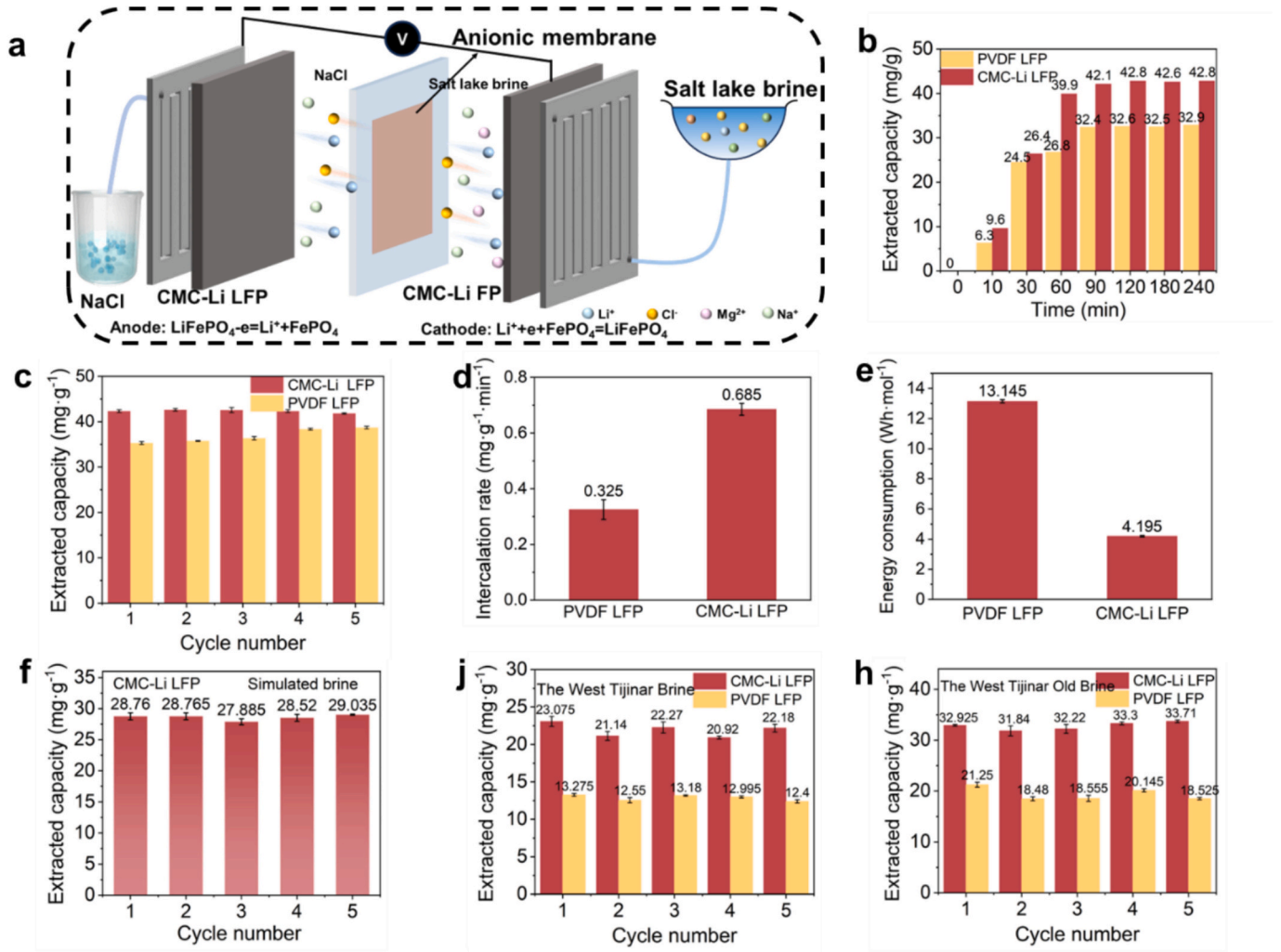

Fig. 6. The Extraction of lithium properties at CMC-Li LFP/CMC-Li FP and PVDF LFP/PVDF FP electrode system. (a) Mechanism for the intercalation/de-intercalation of Li^+ by the CMC-Li LFP/CMC-Li FP electrode.; (b)Relationship between de-lithiation capacity and time ; (c) Lithium extraction capacity after five cycles in 0.1 M LiCl ; (d)Li^+ intercalation rate during the lithium extraction process ; (e)Energy consumption during the lithium extraction process ; (f) Lithium extraction capacity after five cycles in simulated brine ; (j) Lithium extraction capacity after five cycles in the west Tijinar brine ; (h) Lithium extraction capacity after five cycles in the west Tijinar old brine.

mass of Li [6.941 g·mol^{-1}]; U is the applied voltage in the process of external voltage driving [V]; I is the current [A] value; t is the operation time [s]; E_{Li} is the extraction amount of Li [mg·g^{-1}]; W is the mass of LFP [g] [17].

The lithium-extraction efficiency and ion selectivity of this system in artificial brine, the West Taijinar brine, and the West Taijinar old brine was studied. (The concentration of each ion in the simulated brine, the West Taijinar brine, and the West Taijinar old brine is shown in **Table S1**, **Table S2**, and **Table S3**, respectively [28,29].) The lithium-extraction performance in simulated brine is shown in Fig. 6f. The average lithium de-intercalation capacity of the negative electrode was 28.43 mg·g^{-1}, while the average lithium extraction capacities for the West Taijinar brine, and the West Taijinar old brine were 23.01 mg·g^{-1}and 32.79 mg·g^{-1}, respectively (Fig. 6j-h). Compared to PVDF LFP, this demonstrates a significant improvement in lithium extraction capacity. To further evaluate the cyclic stability of the CMC-Li LFP electrode, multiple cycling tests were carried out in raw salt-lake brine. As illustrated in **Fig. S6**, the CMC-Li LFP electrode demonstrates enhanced lithium extraction capacity retention (96.6 %) compared to the PVDF LFP counterpart. Moreover, as shown in **Fig. S7**, the CMC-Li LFP electrode exhibits a significantly lower mass loss (1.14 %) after cycling compared to its PVDF LFP counterpart (4.32 %). Additionally, an ultrasonic treatment experiment performed in brine on the cycled electrode showed almost no active material detachment (**Fig. S8**), indicating excellent structural integrity and adhesion strength. These results collectively demonstrate the outstanding stability of the CMC-Li LFP electrode in realistic brine environments.

Furthermore, we specifically investigated the separation efficiency between Li + and competing ions (Na^+, K^+, Mg^{2+}) in CMC-Li LFP and PVDF LFP systems. As shown in **Fig. S9**, compared to the original brine composition, K^+ was virtually undetectable, while the Mg/Li and Na/Li ratios were significantly reduced relative to PVDF LFP (In the West Taijinar old brine, the Mg/Li ratio decreased from 61.7 to 0.47, Na/Li ratio from 3.42 to 0.28; In the West Taijinar brine, the Mg/Li ratio dropped from 141 to 0.42, Na/Li ratio from 181 to 4.67). These results demonstrate outstanding selectivity for Li^+ extraction, and the separation factors obtained from these brines indicate the system's applicability to different brine types (**Fig. S10**). This enhanced selectivity stems from the preferential intercalation of Li^+ into the active sites of CMC-Li LFP, effectively preventing the co-intercalation of other impurity ions. These findings indicate that the CMC-Li LFP/CMC-Li FP system exhibits outstanding lithium extraction performance and Li^+ selectivity in brine systems.

The above-mentioned research indicates that the CMC-Li LFP/CMC-Li FP system exhibits excellent applicability, stability, lithium extraction efficiency, and lithium- ion selectivity in brines with high viscosity and a high Mg/Li ratio. As depicted in Fig. 7, the diffusion process of the thick electrode in brine is predominantly governed by the interfacial dehydration and internal diffusion stages. When the electrode comes into contact with the brine, an electric double-layer structure is formed at the interface between the electrode particles and the liquid surface [20,30]. In the CMC-Li LFP system, the anionic -COOH and -OH groups attract water-solvated Li^+ ions, altering the charge distribution within the Inner Helmholtz Plane (IHP). According to literature reports, surfaces with negative charge density weaken the interaction between Li^+ and H_2O. The adsorption of anions reduces the hydration of Li^+, decreasing the dehydration free energy from −483 kJ·mol^{-1} to −236.6 kJ·mol^{-1} [20,31,32]. This accelerates Li^+ transport kinetics (reducing Rct by 80.9 %). Furthermore, according to the electric double layer capacitance in **Eq. (3)**.

$$C = \frac{\varepsilon \varepsilon_0 A}{d} \tag{3}$$

where ε represents the relative permittivity of the electrolyte, ε_0 is the vacuum permittivity (8.85 × 10^{-12} F·m^{-1}), A (ECSA) is the effective surface area of the electrode (m^2), and d is the thickness of the electric double layer [24]. Among them, wettability determines the efficiency of brine reaching the active sites of the film electrode, thereby directly affecting the practical effective electrochemical active surface area (ECSA). Compared to the conventional hydrophobic PVDF binder, the modified film electrode exhibits enhanced brine wettability (contact angle of 55.17°), effectively increasing the electrochemical active surface area (ECSA). Furthermore, the Rct, n, Q, and C values obtained from EIS equivalent circuit fitting (**Table S4**) demonstrate that surface charge modification significantly enhances the electric double-layer capacitance, facilitates ion diffusion within the electrode, and consequently improves lithium extraction performance.

2.4. Study on the selectivity of CMC-Li LFP/CMC-Li FP system to impurity ion

The complex composition of Chinese salt lake brine, characterized by low lithium concentration and high levels of impurity ions, poses significant challenges for lithium extraction. According to the above research, in brine with low Li concentration and high Mg/Li, the similar ionic radii of Mg^{2+} and Li^+ (0.72 Å and 0.76 Å) induce competitive adsorption on electrode materials, while the exceptionally high Na^+ concentration (typically 10^3–10^4 mg·L^{-1}) imposes additional interference on lithium-ion selective extraction processes. Therefore, the separation effects of the system on Li^+, Na^+ and Mg^{2+} were respectively

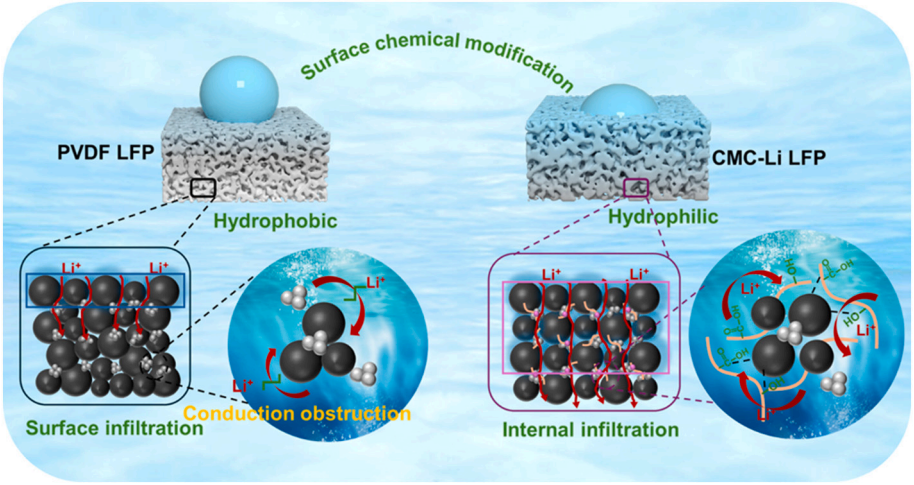

Fig. 7. Diffusion mechanism diagram of CMC-Li LFP in film electrode.

studied by simulating solutions with high Mg/Li and Na/Li. Firstly, to demonstrate the impact of CMC-Li on impurity ion migration, we conducted supplementary electrolysis experiments using CMC-Li on pure carbon electrodes in NaCl solution. As shown in **Fig.S11**, the Li^+ stripping content is negligible (0.8 ppm), confirming that this process does not significantly impact the selectivity of CMC-Li LFP. Then, the electrochemical behavior of the CMC-Li LFP electrode in a solution with Mg/Li = 65 and Na/Li = 181 was investigated. As shown in Fig. 8a-b, the CMC-Li LFP electrode exhibited distinct intercalation currents for Li^+, Mg^{2+}, Na^+ and other ions. The intercalation potentials of Na^+ and Mg^{2+} were − 0.27 V and − 0.48 V, respectively. During the cation de-intercalation process, except for Li^+ and Na^+, Mg^{2+} did not show an obvious oxidation peak. This is due to the olivine structural channels of $LiFePO_4$ were originally designed for Li^+, and the divalent charge of Mg^{2+} results in strong electrostatic repulsion. Overcoming the significant energy barrier for intercalation prevents reversible redox reactions from occurring. Therefore, controlling the voltage of the electrochemical de-intercalation method at 0.25 V can achieve the selective extraction of Li^+.

Based on the above results, the lithium-extraction performance and selectivity of this system were further studied. As shown in Fig. 8c-d, the average lithium - extraction capacity in a solution with Mg/Li = 65 reached 26.84 $mg{\cdot}g^{-1}$, and the Mg/Li ratio decreased from 65 to 0.13. This indicates that when an appropriate potential is controlled, the CMC-Li LFP/CMC-Li FP system has good Li^+ selectivity. This is because the extra Li^+ in CMC-Li occupies the active sites of the electrode, reducing the intercalation of Mg^{2+}. In addition, in a solution with Na/Li = 181, the average lithium- extraction capacity was 25.013 $mg{\cdot}g^{-1}$, and the Na/Li ratio decreased from 181 to 3.2 (Fig. 8e-f). Compared with the pristine LFP, the Na/Li ratio was significantly reduced, though residual Na^+ deintercalation was still observed. This phenomenon arises because while $LiFePO_4$ exhibits excellent Li^+ selectivity when Na^+ and Li^+ concentrations are comparable (due to differences in their ionic radii and intercalation potentials), the extremely high Na^+ concentration in authentic brine leads to partial Na^+ co-intercalation under kinetic control [33]. In addition, the separation coefficients of Mg^{2+} and Li^+ for the CMC-Li LFP/CMC-Li FP system in solutions with different concentrations are shown in Fig. 8j, indicating that the CMC-Li LFP/CMC-Li FP system has good applicability in brines with a high Mg/Li ratio.

To further evaluate the stability of CMC-Li within the $LiFePO_4$ electrode, we first conducted multiple cycling tests in a Mg/Li solution to assess potential interference from Li^+ ions released by CMC-Li itself. As shown in **Fig. S12**, the electrode demonstrated highly stable lithium extraction performance over 40 cycles, with a capacity retention rate of 94.9 %. No increase in Li^+ content was observed, indicating that Li^+ leaching from CMC-Li has a negligible impact on the electrode's performance. Subsequently, we performed additional stability tests on the CMC-Li LFP electrode after repeated lithium extraction cycles. The

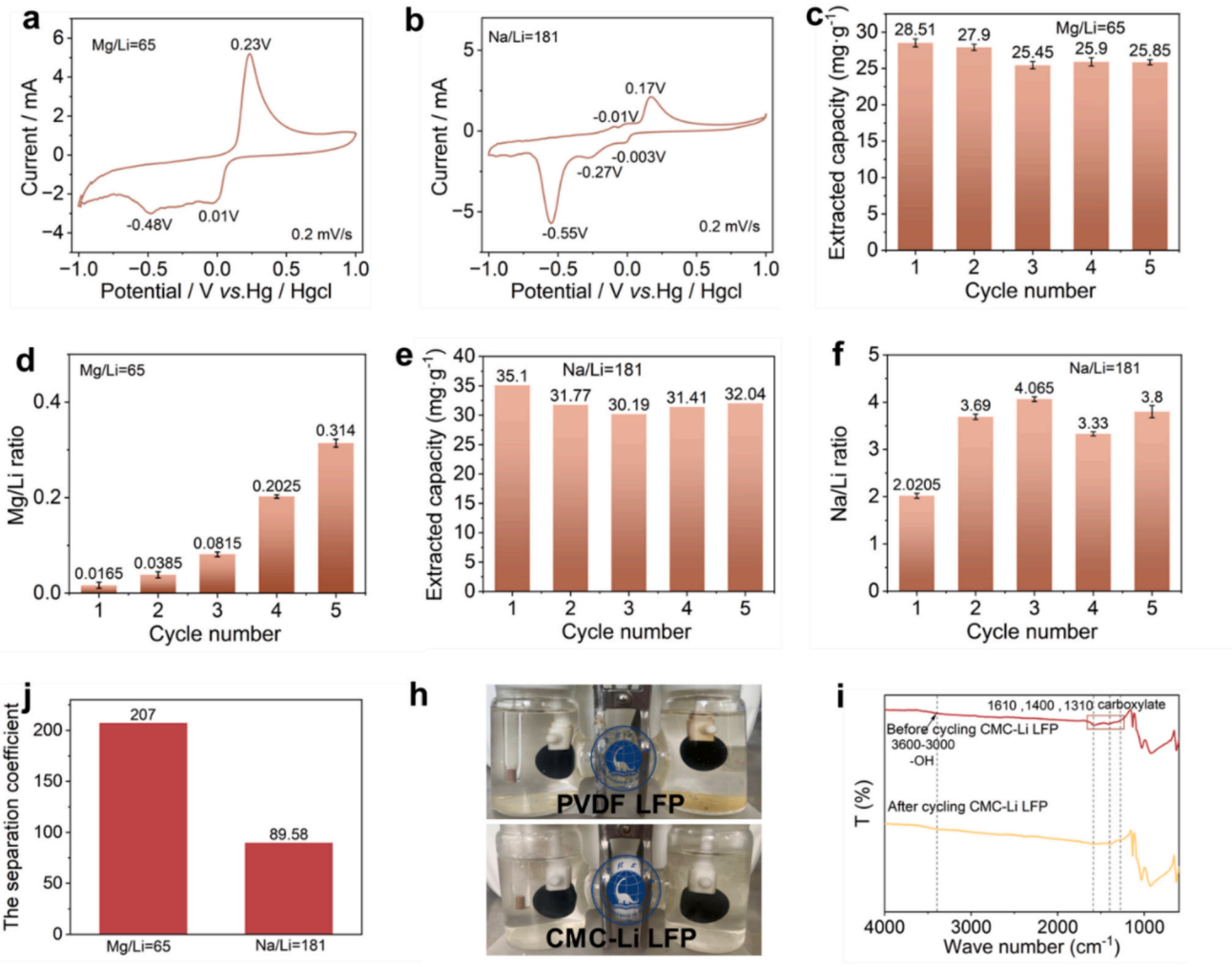

Fig. 8. Circular voltametric test curve of CMC-Li LFP/CMC-Li FP by oxidation method at 0.2 $mV{\cdot}s^{-1}$. (a)Mg/Li = 65; (b)Na/Li = 181; (c)Lithium extraction capacity after five cycles in the solution with Mg/Li = 65; (d)Mg/Li ratio in the solution with Mg/Li = 65; (e)Lithium extraction capacity after five cycles in the solution with Na/Li = 181; (f)Na/Li ratio in the solution with Na/Li = 181; (j)Separation factor; (h)Electrodes after circulation; (i)Infrared spectra of electrodes after cycling.

results further confirm the robustness and durability of the electrode under operating conditions. The CMC-Li LFP electrode sheet after cycling did not show powder-falling or swelling phenomena (Fig. 8h). The functional-group structures of CMC-Li LFP after 10 cycles were consistent with those before cycling, without the appearance of other structures (Fig. 8i), indicating that CMC-Li has good stability. In addition, the XPS spectra before and after cycling, as shown in **Fig. S13 and S14**, both showed the Li 1 s peak, and the Li content before and after cycling was comparable, indicating that when the CMC-Li FP electrocde intercalates Li, the Li in the brine basically occupies the Li sites in the structure. After cycling, the CMC-Li LFP exhibits a Na 1 s peak, which corresponds to the content of Na in the electrode before and after cycling shown in **Fig. S15**. This indicates that a small amount of Na^+ will intercalate into the CMC-Li LFP electrode. This phenomenon requires further investigation in the later stage.

The above results indicate that the regulation of the electric double layer by CMC-Li can significantly increase the contact area between the brine and the film electrode. This not only improves the porosity and specific surface area of the film electrode but also enhances its hydrophilicity. Therefore, the lithium extraction performance is remarkably enhanced. Furthermore, a comparative analysis was conducted between this work and existing studies in terms of hydrophilicity and lithium extraction performance (**Fig. S16)** [13,15–17,34]. The results demonstrate that our approach achieves a significant improvement in lithium extraction efficiency while effectively enhancing surface wettability. Furthermore, in comparison to other hydrophilicity studies, those studies typically accelerate Li^+ transport by introducing a hydrophilic group—this group interacts electrostatically with the positively charged hydrogen atoms in water molecules, thereby enhancing brine wettability. In contrast, while also incorporating hydrophilic groups, this work proposes a novel mechanistic explanation, regulating the electric double layer interface between the film electrode and brine to facilitate Li^+ mass transfer. This provides valuable insights for this field.

3. Conclusions

In summary, this work, from the perspective of the electric double layer, demonstrated that the introduction of CMC-Li can effectively increase the contact area between the brine and the film electrode, thereby enhancing the diffusion process of lithium ions within the film electrode and improving the lithium-extraction efficiency. Experiments confirmed that the thick electrode (approximately 18.8 $mg{\cdot}cm^{-2}$) using CMC-Li as a binder has good lithium extraction performance (23.01 $mg{\cdot}g^{-1}$) and Li^+ selectivity, with the Mg/Li ratio decreasing from 141 to 0.42. Moreover, compared with traditional film electrodes, it significantly improved the lithium-extraction rate (0.69 $mg{\cdot}g^{-1}{\cdot}min^{-1}$) and energy consumption (4.195 $Wh{\cdot}mol^{-1}$). This study provides valuable insights for lithium extraction using thick electrodes via the electrochemical de-intercalation method.

CRediT authorship contribution statement

Yawen Gao: Writing – original draft, Investigation, Formal analysis, Data curation, Conceptualization. **Luxiang Ma:** Writing – review & editing, Investigation, Funding acquisition, Formal analysis, Data curation. **Xin Zeng:** Writing – original draft, Formal analysis. **Zhixiang Li:** Visualization, Formal analysis. **Ting Li:** Visualization, Formal analysis. **Chunxi Hai:** Writing – review & editing, Formal analysis. **Tiandong Chen:** Visualization, Formal analysis. **Yanxia Sun:** Writing – original draft, Formal analysis. **Shengde Dong:** Writing – original draft, Formal analysis. **Xin He:** Writing – original draft, Formal analysis. **Qi Xu:** Writing – original draft, Formal analysis. **Xiaowang Wu:** Visualization, Funding acquisition. **Hongli Su:** Writing – original draft, Formal analysis. **Yuan Zhou:** Writing – original draft, Funding acquisition, Formal analysis.

Experimental

The specific experimental procedures and instrumental characterization are described in the supporting Information.

Declaration of competing interest

The authors declare that we do not have any commercial or associative interest that represents a conflict of interest in connection with the work submitted entitled “Efficient lithium extraction from salt lakes brine via regulating the electric double-layer interface of high-loading film electrodes with CMC-Li”.

Acknowledgements

This research received funding from the Haixi Science and Technology planning Project, under Grant No. 2024-JC-Q01.

Appendix A. Supplementary data

Supplementary data to this article can be found online at https://doi.org/10.1016/j.desal.2025.119395.

Data availability

The used data will be provided as required.

References

[1] F. Maisel, C. Neef, F. Marscheider-Weidemann, N.F. Nissen, A forecast on future raw material demand and recycling potential of lithium-ion batteries in electric vehicles, Resour. Conserv. Recycl. 192 (2023) 106920, https://doi.org/10.1016/j.resconrec.2023.106920.
[2] B.K. Pramanik, M.B. Asif, R. Roychand, L. Shu, V. Jegatheesan, M. Bhuiyan, F. I. Hai, Lithium recovery from salt-lake brine: impact of competing cations, pretreatment and preconcentration, Chemosphere 260 (2020) 127623, https://doi.org/10.1016/j.chemosphere.2020.127623.
[3] D. Fuentealba, C. Flores-Fernández, E. Troncoso, H. Estay, Technological tendencies for lithium production from salt lake brines: Progress and research gaps to move towards more sustainable processes, Res. Policy 83 (2023) 103572, https://doi.org/10.1016/j.resourpol.2023.103572.
[4] B. Swain, Recovery and recycling of lithium: a review, Sep. Purif. Technol. 172 (2017) 388–403, https://doi.org/10.1016/j.seppur.2016.08.031.
[5] Y. Yang, S. Bi, F. Wang, X. Pan, T. Yang, S. Hu, S. Tang, Q. Jia, Solid membrane-based aqueous lithium extraction and adsorption: advances, challenges, and prospects, Chem. Eng. J. 510 (2025) 161748, https://doi.org/10.1016/j.cej.2025.161748.
[6] M. Awais Ashraf, M. Usman, I. Hussain, F. Ahmad, S. Guo, L. Zhang, Lithium extraction from high magnesium salt lake brine with an integrated membrane technology, Sep. Purif. Technol. 302 (2022) 122163, https://doi.org/10.1016/j.seppur.2022.122163.
[7] J. Zhang, T. Chen, L. Ma, C. Hai, Y. Sun, S. Dong, X. He, Q. Xu, J. Chen, H. Su, Y. Zhou, Factors affecting the efficiency of electrochemical lithium extraction: a systematic review from materials to processes technology, Desalination 602 (2025) 118570, https://doi.org/10.1016/j.desal.2025.118570.
[8] Y. Chen, H. Zhan, Y. Qiao, Z. Qian, B. Lv, Z. Wu, Z. Liu, Facet dependent ion channel of iron phosphate for electrochemical lithium extraction, Chem. Eng. J. 477 (2023) 147136, https://doi.org/10.1016/j.cej.2023.147136.
[9] W. Xu, L. He, Z. Zhao, Lithium extraction from high Mg/Li brine via electrochemical intercalation/de-intercalation system using LiMn2O4 materials, Desalination 503 (2021) 114935, https://doi.org/10.1016/j.desal.2021.114935.
[10] K. Shin-mura, K. Sasaki, E. Niwa, S. Honda, H. Tazoe, Voltage effects on lithium extraction/recovery via electrochemical pumping using a La0.57Li0.29TiO3 electrolyte, sustainable Mater. Technol, Sustain. Mater. Technol. 39 (2024) e00779, https://doi.org/10.1016/j.susmat.2023.e00779.
[11] H. Zheng, J. Li, X. Song, G. Liu, V.S. Battaglia, A comprehensive understanding of electrode thickness effects on the electrochemical performances of Li-ion battery cathodes, Electrochim. Acta 71 (2012) 258–265, https://doi.org/10.1016/j.electacta.2012.03.161.
[12] J. Wu, Z. Ju, X. Zhang, X. Xu, K.J. Takeuchi, A.C. Marschilok, E.S. Takeuchi, G. Yu, Low-tortuosity thick electrodes with active materials gradient Design for Enhanced Energy Storage, ACS Nano 16 (3) (2022) 4805–4812, https://doi.org/10.1021/acsnano.2c00129.
[13] J. Zhang, Y. Zhou, C. Hai, H. Su, Y. Zhao, Y. Sun, S. Dong, X. He, Q. Xu, T. Chen, J. Xiang, S. Huang, L. Ma, Enhancing lithium extraction efficiency from salt lake brines through three-dimensional conductive network-incorporated thick

electrodes, Sep. Purif. Technol. 334 (2024) 126010, https://doi.org/10.1016/j.seppur.2023.126010.
[14] J. Zhang, Y. Zhou, C. Hai, Y. Gao, Y. Zhao, Y. Sun, S. Dong, X. He, Q. Xu, J. Chen, H. Su, L. Ma, Constructing the 3D-conductive network-incorporated thick electrodes via melamine foam for lithium extraction, Desalination 579 (2024) 117457, https://doi.org/10.1016/j.desal.2024.117457.
[15] W. Xu, D. Liu, X. Liu, D. Wang, L. He, Z. Zhao, Highly selective and efficient lithium extraction from brines by constructing a novel multiple-crack-porous LiFePO4/FePO4 electrode, Desalination 546 (2023) 116188, https://doi.org/10.1016/j.desal.2022.116188.
[16] G. Luo, X. Li, L. Chen, J. Gu, Y. Huang, J. Sun, H. Liu, Y. Chao, W. Zhu, Z. Liu, Electrochemical recovery lithium from brine via taming surface wettability of regeneration spent batteries cathode materials, Appl. Energy 337 (2023) 120890, https://doi.org/10.1016/j.apenergy.2023.120890.
[17] J. Zhang, L. Ma, C. Hai, T. Chen, Y. Gao, Y. Xu, W. Pan, J. Chen, Y. Sun, S. Dong, X. He, Q. Xu, X. Wu, C. Quan, H. Su, Y. Zhou, Enhancing hydrophilicity of thick electrodes via sulfonation reaction for lithium extraction from salt lake, Desalination 604 (2025) 118669, https://doi.org/10.1016/j.desal.2025.118669.
[18] L. Jiang, D. Li, X. Xie, D. Ji, L. Li, L. Li, Z. He, B. Lu, S. Liang, J. Zhou, Electric double layer design for Zn-based batteries, Energy Storage Mater 62 (2023) 102932, https://doi.org/10.1016/j.ensm.2023.102932.
[19] H. Cheng, Q. Sun, L. Li, Y. Zou, Y. Wang, T. Cai, F. Zhao, G. Liu, Z. Ma, W. Wahyudi, Q. Li, J. Ming, Emerging era of electrolyte solvation structure and interfacial model in batteries, ACS Energy Lett. 7 (1) (2022) 490–513, https://doi.org/10.1021/acsenergylett.1c02425.
[20] J. Hu, W. Ren, X. Chen, Y. Li, W. Huang, K. Yang, L. Yang, Y. Lin, J. Zheng, F. Pan, The role of anions on the Helmholtz plane for the solid-liquid interface in aqueous rechargeable lithium batteries, Nano Energy 74 (2020) 104864, https://doi.org/10.1016/j.nanoen.2020.104864.
[21] D.O. Shin, H. Kim, S. Jung, S. Byun, J. Choi, M.P. Kim, J.Y. Kim, S.H. Kang, Y.-S. Park, S.Y. Hong, M. Cho, Y.-G. Lee, K. Cho, Y.M. Lee, Electrolyte-free graphite electrode with enhanced interfacial conduction using Li+−conductive binder for high-performance all-solid-state batteries, Energy Storage Mater 49 (2022) 481–492, https://doi.org/10.1016/j.ensm.2022.04.029.
[22] H. Zhang, J. Tian, X. Cui, J. Li, Z. Zhu, Highly mesoporous carbon nanofiber electrodes with ultrahigh specific surface area for efficient capacitive deionization, Carbon 201 (2023) 920–929, https://doi.org/10.1016/j.carbon.2022.10.002.
[23] J. Lee, H. Lee, C. Bak, Y. Hong, D. Joung, J.B. Ko, Y.M. Lee, C. Kim, Enhancing hydrophilicity of thick electrodes for high energy density aqueous batteries, Nano-Micro Letters 15 (1) (2023) 97, https://doi.org/10.1007/s40820-023-01072-y.
[24] R.W. Haid, X. Ding, T.K. Sarpey, A.S. Bandarenka, B. Garlyyev, Exploration of the electrical double-layer structure: influence of electrolyte components on the double-layer capacitance and potential of maximum entropy, Curr. Opin. Electrochem. 32 (2022) 100882, https://doi.org/10.1016/j.coelec.2021.100882.
[25] L. Xu, Y. Xiao, Z.-X. Yu, Y. Yang, C. Yan, J.-Q. Huang, Revisiting the electrochemical impedance spectroscopy of porous electrodes in Li-ion batteries by employing reference electrode, Angew. Chem. Int. Ed. 63 (41) (2024) e202406054, https://doi.org/10.1002/anie.202406054.
[26] J. Zhang, W. Su, B. Yi, Y. Guo, T. Deng, X. Yu, A new strategy for the preparation of highly stable and high-capacity electrodes for green electrochemical extraction of lithium, Chem. Eng. J. 454 (2023) 140416, https://doi.org/10.1016/j.cej.2022.140416.
[27] S. Fang, K. Guan, A. Zhang, L. Dai, S. Zhou, W. Fu, M. Hu, P. Xu, P. Zhang, Z. Li, Z. Mai, H. Matsuyama, Multifunctional role of surfactant in fabricating polyamide nanofiltration membranes for Li+/Mg2+ separation, Desalination 594 (2025) 118295, https://doi.org/10.1016/j.desal.2024.118295.
[28] T. Ding, M. Zheng, S. Peng, Y. Lin, X. Zhang, M. Li, Lithium extraction from salt lakes with different hydrochemical types in the Tibet plateau, Geosci. Front. 14 (1) (2023) 101485, https://doi.org/10.1016/j.gsf.2022.101485.
[29] C. Zhu, Y. Dong, Z. Yun, Y. Hao, C. Wang, N. Dong, W. Li, Study of lithium exploitation from carbonate subtype and sulfate type salt-lakes of Tibet, Hydrometallurgy 149 (2014) 143–147, https://doi.org/10.1016/j.hydromet.2014.07.006.
[30] J. Luo, L. Xu, Y. Yang, S. Huang, Y. Zhou, Y. Shao, T. Wang, J. Tian, S. Guo, J. Zhao, X. Zhao, T. Cheng, Y. Shao, J. Zhang, Stable zinc anode solid electrolyte interphase via inner Helmholtz plane engineering, Nat. Commun. 15 (1) (2024) 6471, https://doi.org/10.1038/s41467-024-50890-0.
[31] G. Leverick, Y. Shao-Horn, Controlling electrolyte properties and redox reactions using solvation and implications in battery functions: a mini-review, Adv. Energy Mater. 13 (13) (2023) 2204094, https://doi.org/10.1002/aenm.202204094.
[32] C. Lin, X. He, C. Xi, Q. Zhang, L.-W. Wang, Ion solvation free energy calculations based on first-principles molecular dynamics thermodynamic integration, J. Chem. Phys. 160 (18) (2024) 184115, https://doi.org/10.1063/5.0191068.
[33] Y. Gao, L. Ma, S. Zhao, C. Hai, T. Chen, J. Zhang, Y. Zhao, Y. Sun, S. Dong, X. He, Q. Xu, X. Wu, C. Quan, H. Su, Y. Zhou, Cost-effective and efficient preparation of FePO4 electrodes from spent LiFePO4 batteries for enhanced lithium extraction from salt lakes, Materials Today Energy 50 (2025) 101848, https://doi.org/10.1016/j.mtener.2025.101848.
[34] Y. Wang, J. Zhang, Z. Cheng, X. Xiang, Hydrophilic modification using polydopamine on core–shell Li1.6Mn1.6O4@carbon electrodes for lithium extraction from Lake Brine, ACS Sustain. Chem. Eng. 10 (27) (2022) 8970–8979, https://doi.org/10.1021/acssuschemeng.2c02706.